Desalination and Water Treatment
www.deswater.com

doi: 10.5004/dwt.2021.27434

230 (2021) 204–218
August

Synthesis and characterization of crosslinked membranes based on sodium alginate/polyvinyl alcohol/graphene oxide for ultrafiltration applications

Asma Rhimi[a,c], Khira Zlaoui[a,d], Bart Van der Bruggen[b], Karima Horchani-Naifer[a], Dorra Jellouli Ennigrou[a,*]

[a]*Physical Chemistry Laboratory of Mineral Materials and their Applications, National Center for Research in Materials Sciences, Technopark Borj Cedria, P.O. Box: 73-8027, Soliman, Tunisia, Tel. (+216) 79 32 52 50/(+216) 79 32 52 80; emails: ennigrou2@gmail.com (D.J. Ennigrou), asmarhimi2014@gmail.com (A. Rhimi), khira.zlaoui@gmail.com (K. Zlaoui), karima_horchani@yahoo.com (K. Horchani-Naifer)*
[b]*Department of Chemical Engineering, KU Leuven, Celestijnenlaan 200F, B-3001, Leuven, Belgium, email: bart.vanderbruggen@kuleuven.be*
[c]*Faculty of Sciences of Tunis, Tunisia*
[d]*Faculty of Sciences of Bizerte, Tunisia*

Received 9 March 2021; Accepted 9 May 2021

ABSTRACT

Novel sodium alginate/polyvinyl alcohol/graphene oxide (SA/PVA/GO) nanocomposite ultrafiltration membranes were successfully synthesized via the phase inversion process. Their application in ultrafiltration requires crosslinking. The resulting hydrophilic membranes were *in situ* crosslinked using glutaraldehyde as a covalent crosslinker and calcium chloride as an ionic crosslinker. The synthesized membranes were characterized using differential scanning calorimetry, X-ray diffraction, water contact angle, scanning electron microscopy and Fourier-transform infrared spectroscopy. Performance tests showed that the sodium alginate membranes have a high affinity for bovine serum albumin and can remove 87% at an optimum transmembrane pressure of 2 bar. The presence of GO improved the cobalt and copper rejection, reaching around 23% (Co) and 34% (Cu) at 2 bar. The prepared membrane showed a higher affinity for Cu^{2+} than for Co^{2+} due to the size effect. The permeability of the membranes was improved by increasing the PVA concentration up to 3 wt.%. The use of graphene oxide increased the hydrophilic property of the membrane, which yielded a significantly higher flux than the unmodified membrane. The as-prepared membrane with 3 wt.% SA, 9 wt.% PVA, and 0.3 wt.% GO percentages was chosen as the best membrane and was found to have the optimal performance.

Keywords: Membrane; Sodium alginate; Glutaraldehyde; Chloride calcium; Ultrafiltration; Covalent and ionic crosslinker

1. Introduction

Pollution of water by various toxic chemicals such as dyes, organics and heavy metals is a global problem due to the high toxicity of these elements and their tendency to accumulate in living organisms through the food chain, affecting public health [1–3].

Non-biodegradable metal ions are one of the most significant water pollutants. For example, copper and cobalt, essential nutrients in trace amounts, can produce health problems when they are present at a high level [4,5]. Therefore, methods for removing copper and cobalt ions from wastewater are of great significance. At present, various approaches are used for the removal of heavy metals from effluents, such as the ion exchange [6] membrane filtration [7], solvent extraction [8] and adsorption [9,10].

* Corresponding author.

Among these methods, filtration using biopolymer membranes, such as alginate, has been proven to be a promising technology to remediate heavy metals from wastewater due to its simple operation, high efficiency, availability of different polymers, and low cost [10,11].

The popularity of synthetic polymers has recently decreased due to their non-environmental compatibility and degradability [12]. The use of natural polysaccharides, especially alginate, for various applications has drastically increased. Alginate is a hydrophilic naturally occurring anionic heteropolysaccharide, soluble in water, made up of two monomeric units: (1,4)-β-D-mannuronic acid (M) residues and (1,4)-α-L-guluronic acid (G) residues (Fig. 1). The basic structure of alginate consists of linear, unbranched units of polymers made of monomers arranged in blocks of M and G residues interspersed with regions containing an alternating M-G sequence within the structure [13,14].

Different varieties of alginate contain varying ratios of M and G. Depending on the arrangement of the varying M, G, or MG blocks, alginate copolymers of slightly different behaviors and properties can be produced [15]. Marine biological resources, especially brown seaweed species, produce it abundantly and sustainably. The physical and biochemical structure of alginate enables it to have great potential in various fields; it has been widely applied in the food industry [16], in pharmaceutical products [18], in environmental applications, and for water purification.

Alginate is used in different forms, such as films, microspheres, fibers [17], and composite membranes. It is considered non-toxic, biodegradable [18,19], biocompatible [20], and renewable [21,22]. Furthermore, it is easy to modify chemically, relatively cheap [23,24] and undergoes gelation in the presence of divalent cations through ionic interaction.

The great interest of this family of polysaccharides is mostly related to the gelling properties. An important property of sodium alginate (SA) is its ability to be used as a gelling agent [25]. This is due to its mild gelation by the addition of divalent cations such as Ca^{2+} to form a highly compacted and dense gel network [26] independently of temperature as compared to other polysaccharides [23,24].

Many divalent cations were found to induce alginate gelation [27,28]. The most interesting cation that has been widely used to prepare crosslinked alginate membranes is calcium [27,29].

The addition of calcium ions into the alginate polymer causes the binding of two guluronate G-chains on opposite sides to form hydrogels [30,31]. Calcium chloride ($CaCl_2$) is one of the most frequently used agents to crosslink ionic alginate (Fig. 2).

SA is rich in the foremost groups involved in heavy metal retention, that is, hydroxyl (OH) and carboxyl (COOH) functional groups and extra negatively charged sites [32].

Conventional cross-linkers were also examined to develop alginate membranes. Glutaraldehyde is the most common cross-linker [33,34]. Glutaraldehyde has had great success thanks to its commercial availability, low cost and high reactivity. It reacts rapidly with amine groups at around neutral pH and is more efficient than other aldehydes in generating thermally and chemically stable crosslinks [35].

Among the treatment methods, ultrafiltration attracts more attention due to its high efficiency in treating low-concentration wastewater, low cost, simple operation, compactness, and energy efficiency.

In this context, the use of membranes composed of natural polymers, such as sodium alginate appears to be an eco-friendly and efficient alternative for membrane filtration of solutions containing copper and cobalt. Investigations of alginate membranes for applications in water treatment have drastically increased [10]. In recent pioneering works, alginate is used as a membrane material [11]. Subsequently, several studies on the synthesis of sodium alginate membranes have been carried out [36–40]. Sodium alginate leads to hydrophobic membranes; however, the composition of the membrane can be modified in order to obtain a more hydrophilic material. Therefore, recent studies focus on the addition of hydrophilic additives such as polyvinyl alcohol (PVA) and graphene oxide (GO) [41,42].

PVA is a non-toxic, biodegradable and highly hydrophilic synthetic polymer containing pendant hydroxyl groups and its aqueous solution can form transparent films. However, it is not soluble in cold water and must be heated at temperatures above 90°C. It is a nonionic surfactant, used in many areas of science and technology, including membrane separation [43–45]. PVA contains a large number of (–OH) groups, which can be a source of hydrogen bonding and therefore contribute to the formation of transparent membranes Many efforts have been made to enhance the performance of alginate membranes by blending it with different hydrophilic polymers. PVA is

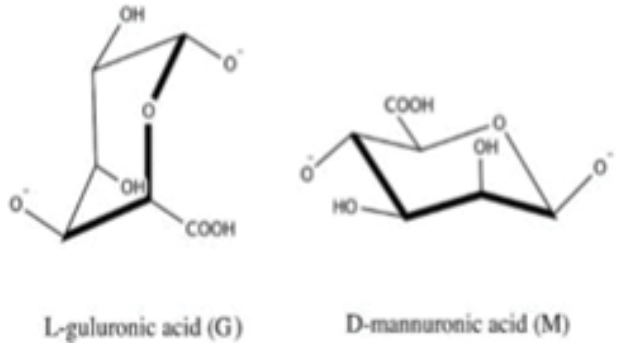

Fig. 1. Chemical structure of alginate monomers: L-guluronic acid and D-mannuronic acid.

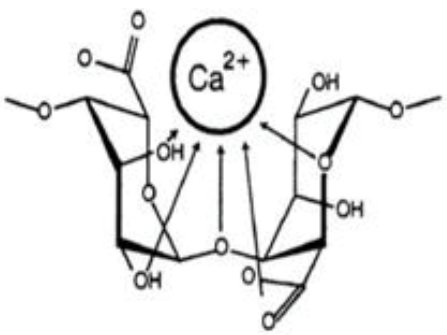

Fig. 2. Calcium alginate net formation.

a common polymer for a variety of applications in water treatment. PVA membranes show a lower permselectivity and higher permeability due to their hydrophilicity [46].

Graphene oxide (GO) is a new carbon material with excellent properties such as high hydrophilicity, low toxicity, chemical, and biological durability, and antibacterial properties, which make GO a very good nanomaterial for the development of hydrophilic membranes [47].

The combination PVA-SA is stronger than SA alone, which confirms its excellent water rejection [48].

The aim of this work is to prepare sodium alginate membranes crosslinked with calcium chloride ($CaCl_2$) and glutaraldehyde (GrA) for use in ultrafiltration to retain proteins such as bovine serum albumin and heavy metals such as cobalt and copper. PVA and GO might enhance the physicochemical properties of SA and optimize its performance.

2. Materials and methods

2.1. Chemicals and materials

Sodium alginate (SA, M_w = 35.000 g mol^{-1}) was supplied from Sigma-Aldrich (Germany). Glutaraldehyde ($C_5H_8O_2$) 25% solution (M_w = 100.12 g mol^{-1}, d = 1.130) was purchased from PROLABO. Calcium chloride anhydrous ($CaCl_2$ ≥ 96 wt.%) and isopropanol alcohol (IPA, D_s = 0.79) were purchased from Chem Lab. Polyvinyl alcohol PVA (M_w ~~ 72,000 g mol^{-1}) was purchased from Chemica (Germany). Bovine serum albumin (BSA, M_w ~ 66 kDa, P ≥ 96%) was purchased from Chemica (Germany).

Copper(II) nitrate trihydrate ($CuN_2O_6{\cdot}3H_2O$) (M_w = 241.6 g mol^{-1}) and cobalt(II) nitrate hexahydrate ($CoN_2O_6{\cdot}6H_2O$) (M_w = 291.03 g mol^{-1}) were purchased from Sigma-Aldrich (Germany) and were used for the evaluation of the membrane performance. Graphene oxide was purchased from Sixth Element Materials Technology, Changzhou, China, and all the aqueous solutions were prepared with ultrapure water.

2.2. Preparation of SA/PVA/GO membranes

M, M1, M2 and M3 membrane solutions are shown in Table 1.

A solution of sodium alginate with concentration ranging from 1.0 to 7.0 wt.% was prepared by dissolving the mass of sodium alginate in ultrapure water through phase inversion. Then, the solution was mixed by magnetic stirring for about 5 h at room temperature (25°C) to ensure homogeneity. After complete dissolution, the solution was slowly placed in clean Petri dishes with bubble-free and completely dried at room temperature in a fume hood for 3 d. However, drying can be replaced by heating in an oven at 50°C for 24 h followed by vacuum drying at a pressure of 15 Pa. A dried thin film of sodium alginate was obtained on the Petri dish.

Table 1
Formulations of the prepared membrane solutions with SA, PVA, GO with temperature and time of stirring

Solutions	M	M1	M2	M3
UP	*	*	M1	M1
SA (3 wt.%)	*		+	
PVA (3, 6, 9 wt.%)		*	M	
GO (0.3, 0.6, 0.9 wt.%)				*
Temperature of stirring (°C)	25	60	90	70

A concentration of 3 wt.% was chosen as the best membrane solution noted (M) because the gel of SA, in this case, has a medium viscosity denoted as alginate medium viscosity which can be easily removed from the Petri dishes when the gel is thick and gives a high pure water flux.

The resulting membranes were dense. Therefore, some PVA was used as pore former to enhance the hydrophilicity. The membrane thickness was measured with a micrometer.

Three solutions of PVA with the following percentages (3.0, 6.0, 9.0 wt.%) were prepared by dissolving the mass of PVA in ultrapure water. Then, the solutions were heated and stirred at 60°C for 6 h.

A concentration of 9 wt.% was chosen as the best membrane solution, denoted as (M1).

Afterward, the M1 solution was added to the solution (M) in one beaker. After that, it was heated at 90°C and kept under agitation for 2 h to obtain a mixture noted (M2).

After complete dissolution, the solution was poured bubble-free in Petri dishes and dried at room temperature. Graphene oxide with the following percentages (0.3, 0.6 and 0.9 wt.%) was suspended in distilled water using ultrasonication for 3 d and heated at 70°C.

The best mixture of GO, that is, with concentration of 0.3 wt.%, was added to the solution M2 to obtain a mixture denoted as (M3). It was mixed homogeneously in one beaker under magnetic stirring for 48 h and heated at 70°C. This solution was followed by casting onto a clean Petri dish, without bubbles, and allowed to dry in the atmosphere at room temperature.

A schematic diagram describing the synthesis of crosslinked membranes is shown in Fig. 3. The developed membranes must be crosslinked before use in filtration process. A dried, thin membrane of sodium alginate was peeled off the Petri dish and immersed totally at ambient temperature in a reaction solution that contained a certain content (2.5 wt.%) of $CaCl_2$ as a source of divalent cations for crosslinking for a further 2 h; after that, in a GrA solution at 5 wt.% for 5 h. After the crosslinking reaction, stable alginate membranes were quickly formed in the Petri dish at room temperature. They were taken out of the reaction solution, washed-out repeatedly with pure water to remove excess electrolyte and then stored in a solution with 1% $CaCl_2$.

The experiments were followed by the best concentrations (3.0 wt.% of SA, 9.0 wt.% of PVA and 0.3 wt.% of GO). The higher concentrations of GO (0.6 and 0.9 wt.%) were not further considered because the membranes prepared with these concentrations were found to dissolve during the crosslinking process.

Five crosslinked membranes with $CaCl_2$ and GrA were developed for use in ultrafiltration, as shown in Table 2.

These nomenclatures will be used as follows in the whole manuscript: ALG3/ALG3-PVA3/ALG3-PVA6/ALG3-PVA9/ALG3-PVA9-GO0.3.

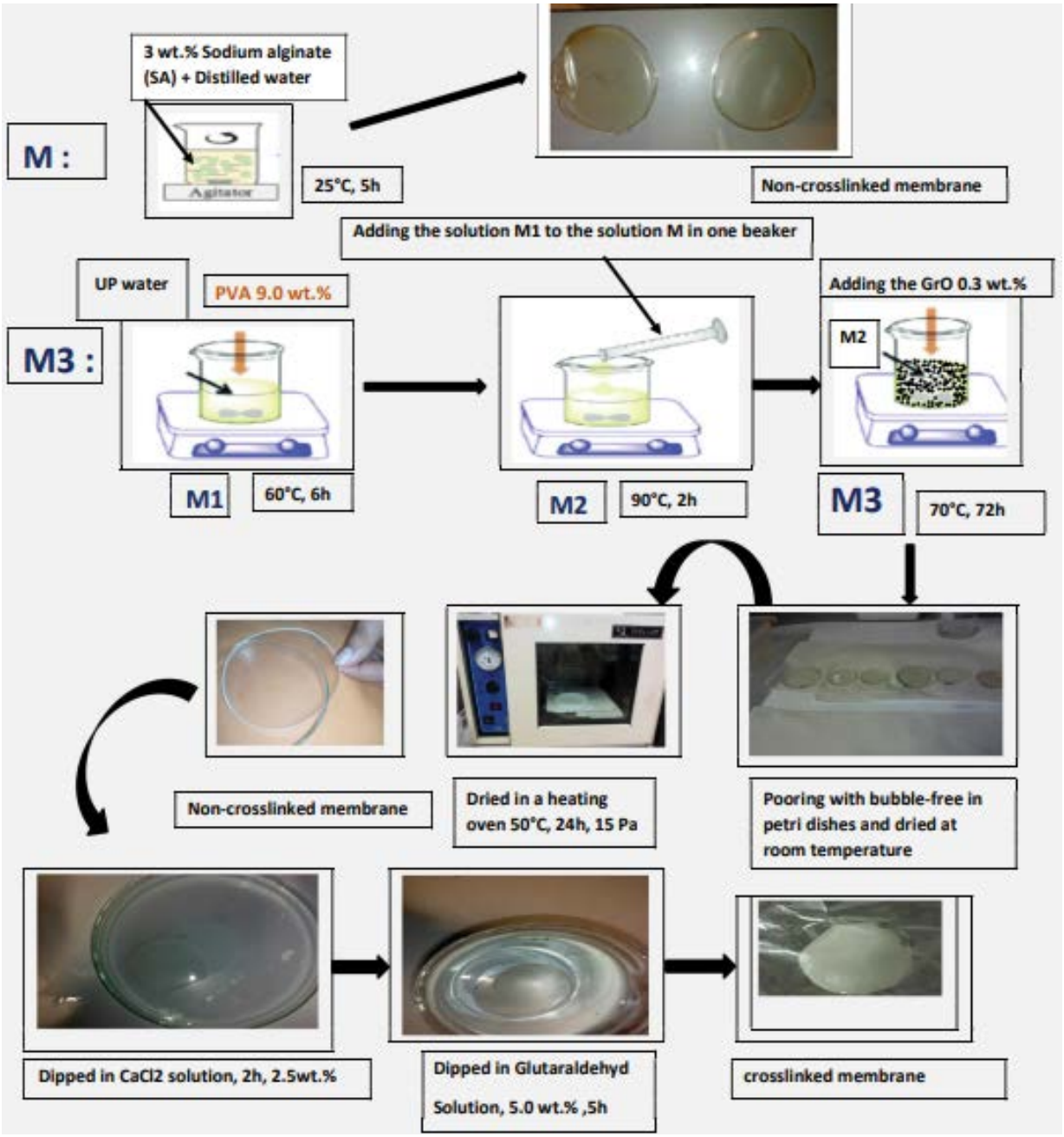

Fig. 3. Preparation of SA/PVA/GO crosslinked membrane with $CaCl_2$ and GrA.

2.3. Membrane characterization

2.3.1. Scanning electron microscopy analysis

The morphology of NaAlg membranes was visualized using a Scanning Electron Microscope Philips XL30 FEG (Eindhoven, The Netherlands).

2.3.2. Thickness

The membrane thickness was measured using a digital micrometer, before (dry state) and after (wet state) the swelling test.

2.3.3. Infrared spectrophotometric analysis

The characterization of the chemical groups of the developed membranes was carried out by Fourier-transform infrared spectroscopy (FTIR) in a Frontier FT-IR/FIR Spectrometer, model Perkin Elmer (France) equipped with, an accessory for working in attenuated total reflectance (ATR) between 400 and 4,000 cm^{-1} at 25°C. It was used to study the reaction between the hydroxyl groups of PVA, the aldehyde groups of glutaraldehyde (GrA) and acetate groups of SA on the membrane and to determine the presence of hydrogen bonds between GO and SA.

Table 2
Developed membranes crosslinked by calcium chloride (2.5 wt.% $CaCl_2$) and glutaraldehyde (5 wt.% GrA)

Membrane designation	SA (wt.%)	PVA (wt.%)	GO (wt.%)
ALG3	3	–	–
ALG3-PVA3	3	3	–
ALG3-PVA6	3	6	–
ALG3-PVA9	3	9	–
ALG3-PVA9-GO0.3	3	9	0.3

2.3.4. Porosity

The porosity of the prepared membranes was determined by a gravimetric method. The membrane porosity (ε_m) was defined as the volume of the pores divided by the total volume of the membrane. It was determined by measuring the weight of IPA contained in the membrane pores:

The porosity of a membrane was calculated by the following Eq. (1):

$$\varepsilon_m = \frac{\left[\left(W_1 - W_2 / D_S\right)\right]}{\left[\left(W_1 - W_2 / D_S\right) + \left(W_2 / D_p\right)\right]} \quad (1)$$

where W_1 is the weight of the wet membrane, W_2 is the weight of the dry membrane, D_S is the solvent density (IPA, 0.79), D is the polymer density.

The reported porosity data are the average values of four samples for each membrane.

As shown by the results of diffusion studies, alginate pores can range from 3.6–14 nm for 4% alginate [49,50] and 3 nm and 14.5–17 nm for 1.5% and 3% alginate, respectively [51].

2.3.5. Contact angle determination

Contact angle measurements of a DI water droplet on the membrane surface were carried out with a contact angle goniometer (OCA20, DataPhysics Instruments, Germany) at room temperature to observe the hydrophilicity changes of the membrane before and after modification with PVA and GO. Before the test, developed membranes were dried overnight in an oven at 50°C. The reported contact angle represents the average water SA values of at least three measurements for each membrane.

2.3.6. X-ray diffraction analysis

A model D8 ADVANCE, Bruker, German of X-ray diffractometer (40 kV, step size 0.015°, 40 mA), at room temperature in the Bragg–Brentano geometry was utilized to characterize the crosslinked and non-crosslinked membrane structure. X-rays of 1.5406 Å wavelengths were generated by a CuK source. The angle of diffraction for 2θ with a scanning rate ranged from 3° to 80° at a velocity of 1 min^{-1}.

2.3.7. Differential scanning calorimetry

Thermal analyses by differential scanning calorimetry (DSC) measurements were carried out on samples over the temperature range of 30°C–500°C using a Mettler Toledo DSC823e. In order to obtain the DSC curves, samples from different membranes were placed in an aluminum crucible, at 10°C/min heating rate.

2.4. Filtration performance experiment

2.4.1. Filtration setup

Ultrafiltration experiments carried out with a dead-end setup (Fig. 4) supplied by Drehzahl Electronic were used to measure water flux and rejections by ultrafiltration. During the filtration, a membrane with an effective area 14.5 cm^2 was applied in the cell. The equipment consisted of a dead-end filtration cell (Fig. 4a), a 3-way valve to be placed on the top of the filtration cell (Fig. 4b) and a nitrogen gas supply (50 bar max) with a pressure regulator (Fig. 4c).

2.4.1.1. Preparation of metal ion solutions

Different concentrations of copper and cobalt ions were prepared by dissolving a certain amount of salt in 500 mL deionized water. To ensure that the salts completely dissolved, the samples were subjected to magnetic

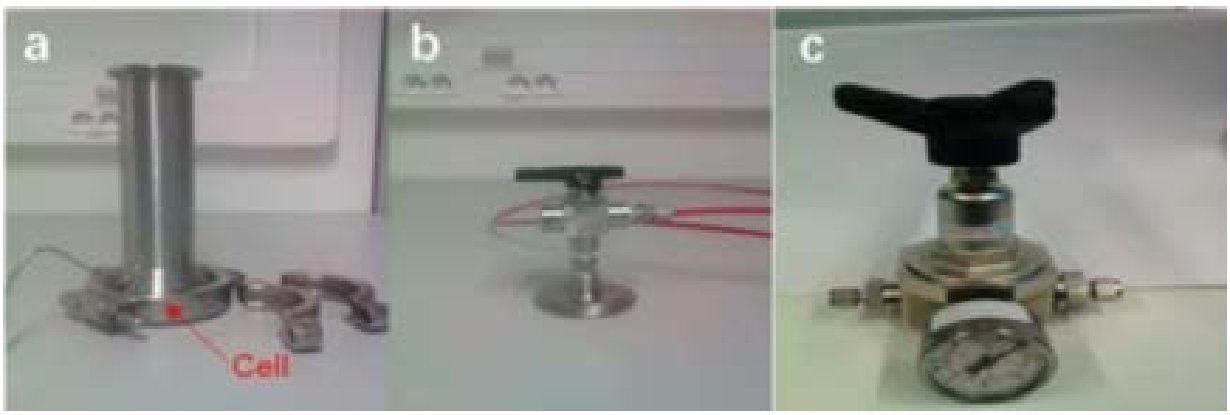

Fig. 4. Picture of filtration unit of the dead-end filtration setup; (a) filtration cell, (b) 3-way valve, and (c) pressure regulator.

stirring (1,000 rpm) for 30 min at room temperature (25°C). The pH of the mixed salt solution was measured to be 5.3. The concentration of the metals in the solution was 1 g L^{-1}.

2.4.1.2. Water flux measurements

Each experiment started at a constant flow rate of 15 mL min^{-1}, with the transmembrane pressure varying from 1 to 6 bar. The ultrafiltration experiments were carried out at room temperature (~25°C). Samples to be analyzed were taken at the inlet (ultrapure water as feed solution) and at the outlet of the system (permeate). The membrane performance was evaluated by measuring the flux of ultrapure water.

The permeation flux J_v (L m^{-2} h^{-1}) was measured by determining the permeate volume produced in a period of time and calculated using the following equation:

$$J_v = \frac{V_p}{(A \times t)} \quad (2)$$

where J_v is the permeate flux (L m^{-2} h^{-1}), V_p (L) represents the volume of the permeate water collected over a period of time t (h) through an effective membrane surface area A (m^2).

The ultrapure water flux through the membrane at one particular transmembrane pressure is usually expressed with Darcy's Law:

$$J_v = \frac{\Delta P_m}{\eta R_m} = Lp^\circ \Delta P_m \quad (3)$$

where Lp° is the permeability of the solvent. It depends on the solvent viscosity (η), and morphological characteristics of the membrane (porosity, specific surface, etc.); ΔP_m is the transmembrane pressure and R_m is the hydraulic membrane resistance.

2.4.1.3. Rejection calculations under transmembrane pressure

Protein solutions were prepared 1 h before use and stored at 4°C to ensure that BSA molecules were active and that there was no bacterial contamination. The feed transmembrane pressure was controlled in the range of 2–6 bar by using compressed nitrogen and the filtration process was carried out by filtering 15 mL of protein solution through the membranes at ambient conditions.

Bovine serum albumin (BSA) was used as a model protein; it was prepared in a concentration of 1 g L^{-1} in a buffered solution (pH = 7). The BSA content in the permeate and feed was analyzed with a UV-Vis Spectrophotometer SF-102 (NPO INTERPHOTOPHYSICS, Moscow, Russia), at 298 nm corresponding to the maximum value for the protein.

The efficiency of the membrane filtration process was determined by the evaluation of the BSA, cobalt, and copper retention coefficients R (%) by means of the following equation.

$$R = \left(1 - \frac{C_p}{C_f}\right) \times 100\% \quad (4)$$

where C_p and C_f are the BSA, cobalt and copper concentrations in the permeate and feed concentration (g L^{-1}), respectively.

3. Results and discussion

3.1. Water flux and protein permeation efficiency

Permeate fluxes of pure water and BSA as a function of transmembrane pressure through the SA membranes are shown in Fig. 5a and b respectively. Permeate fluxes increased when the transmembrane pressure increased from 1 to 6 bar, consistent with Eq. (3). The slopes of the straight lines are the pure water membrane and BSA solution permeabilities respectively shown in Fig. 5a and b.

Table 3 reports the experimental measurements of the ultrapure water, water permeability with BSA solution and correlation coefficients for five crosslinked membranes.

According to Fig. 5a and b, it can be noticed that the variation of flux with the transmembrane pressure obeys Darcy's Law by Eq. (3).

Table 3 shows that the permeability increased with the PVA amount due to the enhancement of the hydrophilicity of the membrane. When a small amount of graphene oxide was added, it had the same effect as the addition of PVA. The presence of GO improved the hydrophilicity of the membrane, which resulted in a higher water flux. Thus, the ALG3-PVA9-GO0.3 membrane was concluded to have the best performance.

3.2. BSA removal

Fig. 6 represents the variation of BSA retention as a function of the transmembrane pressure for a feed protein concentration of 1 g L^{-1} at 25°C. It shows that the BSA retention reached nearly ~87% at 2 bar for the ALG3 membrane. Beyond 2 bar, the rejection of BSA decreased for all membranes and reached 70% at 6 bar. As a consequence, the optimum pressure was taken as 2 bar.

3.3. Metal ions removal

The potential of the SA membrane to remove metal ions was explored for cobalt and copper, using the membrane ALG3-PVA9-GO0.3, which was found to have the highest flux (Table 3). The retention of copper and cobalt ions was calculated by Eq. (4) at 1 g L^{-1} feed concentration. Retentions were 33.7% (Cu) and 23% (Co) at 2 bar.

The difference between these retentions can be explained by molar mass and ionic radius of the two metals that have been considered. The lower Co retention can be attributed to its ionic radius, which is lower than that of Cu ions: the ionic radii of Co^{2+} and Cu^{2+} are 65 and 73 pm, respectively [52]. Ions with larger ionic radius tended to hold their hydration shell and strongly attached to water molecules, and would thus be more removed by the membrane. Thus, copper ions more easily attach to the negatively charged ions of the alginate membrane.

Due to the addition of PVA and GO to sodium alginate, the pore formation invoked by PVA and the hydrophilic nature of GO enhance the ultrapure water permeability and decrease the removal of metal ions.

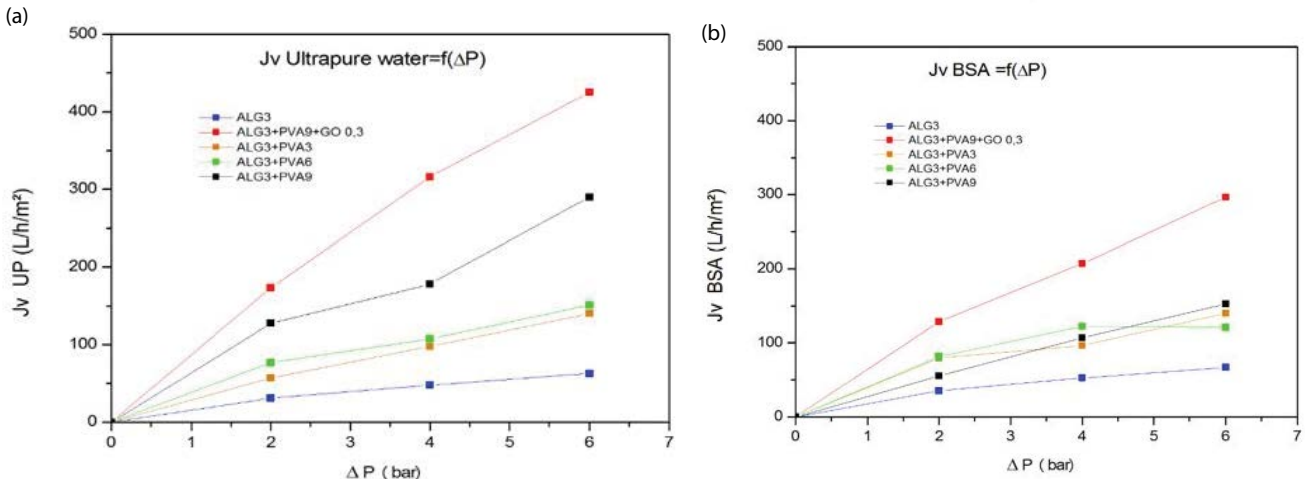

Fig. 5. (a) Permeate fluxes of pure water as a function of transmembrane pressure and (b) permeate flux of BSA as a function of transmembrane pressure, [BSA] = 1 g/L.

Table 3
Water permeabilities of five membranes (measured with ultrapure water) and physical characteristics of alginate membranes

Membrane designation	Contact angle (°C)	Thickness (μm)	Ultrapure water permeability Lp° (L h^{-1} m^{-2} bar^{-1})	Water permeability with BSA solution Lp° (BSA) (L h^{-1} m^{-2} bar^{-1})	R^2 (Ultrapure water)	R^2 (BSA)
ALG3	64.7	0.058	11.3	12.2	0.9511	0.926
ALG-PVA3	47.8	0.047	24	26	0.9903	0.9975
ALG-PVA6	42.7	0.043	26.6	21.5	0.9466	0.7468
ALG-PVA9	41.1	0.036	48.3	24.7	0.9726	0.7663
ALG3-PVA9-GO0.3	37.6	0.028	74.3	51.2	0.9861	0.9828

3.4. Contact angle

The hydrophilicity of biobased membranes can be a very important asset in ultrafiltration. The contact angle measurements of the prepared membranes crosslinked with $CaCl_2$ and GrA (ALG3, ALG3-PVA3, ALG3-PVA6, ALG3-PVA9, and ALG3-PVA9-GO0.3) are shown in Fig. 7.

The hydrophilicity of SA increased with the amount of PVA until 9 wt.%.The contact angle decreased to 41.1°, which led to an increase of permeability [42]. Furthermore, the presence of GO led to a decrease of the water contact angle. The water contact angle decreased to 37.6° and the ALG3-PVA3-GO0.3 membranes showed a good hydrophilicity. This may be because the addition of a small quantity of GO increased the hydrophilicity of the developed membranes. Further consideration was given to the use of 0.3 wt.% GO. The contact angle decreased to 41.1° after adding 9 wt.% of PVA to 3 wt.% of SA. This may be related to the presence of amine and hydroxyl functional groups in the membranes structures. The addition of 0.3 wt.% GO led to a decrease in the contact angle to 37.6°. The decrease of contact angle can be understood by three factors: porosity, pore size and pure water permeation. These factors are the basic properties related to the contact angle of the membrane [53]. This considerable enhancement in membrane hydrophilicity can be attributed to the super hydrophilic nature of GO as a result of the high affinity of GO to water.

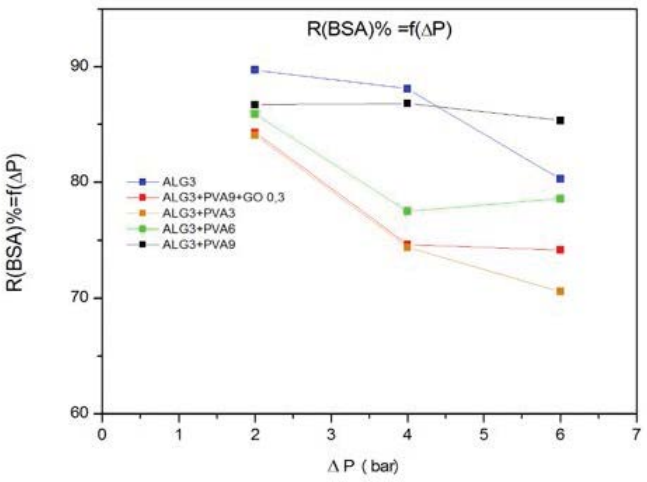

Fig. 6. BSA retention as a function of transmembrane pressure, [BSA] = 1 g/L.

3.5. Scanning electron microscopy analysis

Fig. 8a displays the microstructure of the surface (ALG3) of non-crosslinked membranes. The structure of the non-crosslinked membrane (ALG3) was found to be

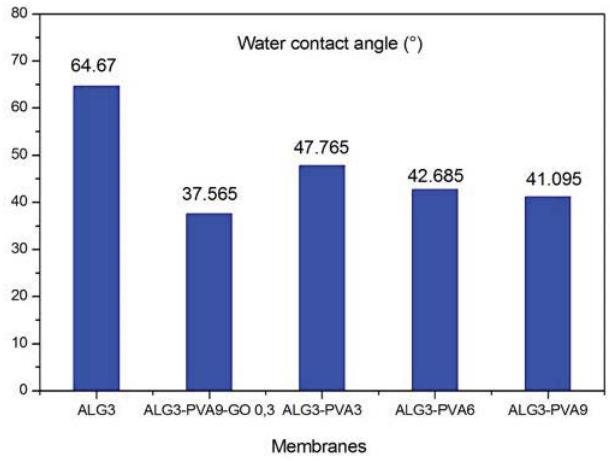

Fig. 7. Water contact angles of sodium alginate (SA) membranes with and without PVA and GO.

smooth, uniform, and flat. It has no pores; the structure of the membrane is homogeneous.

Scanning electron microscopy (SEM) photographs of the ALG3/ALG3-PVA3/ALG3-PVA6/ALG3-PVA9/ALG3-PVA9-GO0.3 crosslinked membranes are shown in Fig. 8b.

Conversely, the crosslinked membranes were observed to have a rougher structure. The addition of different fractions of PVA (3, 6, and 9 wt.%) into the sodium alginate solution created pores at the surface of the membranes. When a high concentration of PVA was added (9 wt.%), the pores diameters increased significantly, as shown in Fig. 8a and b. The surface roughness of the membrane formed with the addition of 3 wt.% PVA appears to be the same as that of the blank. However, for 6 and 9 wt.% the surface becomes more porous and homogeneous. Thereby, no microphase separation and no bulky agglomeration were observed. This illustrates the compatibility between PVA and SA and the good dispersion resulting from the strong interaction between GO and SA.

Upon decreasing the concentration of PVA (3 wt.%), the pore size decreased, because much more molecular chains participated in the crosslinking reaction, leading to the formation of a dense network structure with relatively small pore size. When the concentration of PVA was above 6 wt.%, some large and close pores formed [54].

The change in morphology could be due to the large difference in the homogeneity or hydrophilicity between PVA and SA, which produced significant roughness differences and structural pores [37].

The PVA/SA membrane was found to have a relatively porous structure and small macropores. However, after adding GO, the membrane had a larger and more irregular pore than the PVA/SA membrane.

3.6. X-ray diffraction analysis

Fig. 9a and b show the X-ray diffractograms of non-crosslinked SA membranes and SA membranes crosslinked with $CaCl_2$ and GrA, respectively.

Non-crosslinked and crosslinked SA membranes exhibited different typical diffraction peaks. For the membranes crosslinked with $CaCl_2$ and GrA, the peaks had a high intensity at $2\theta = 20°$ in the ALG3-PVA6, ALG3-PVA9, ALG3-PVA9-GO0.3 membranes. However, the non-crosslinked membranes were almost nonexistent.

When the percentage of PVA was enhanced from 3 to 9 wt.%, the crosslinked SA membranes were observed to have a more compact and rigid structure; this was confirmed by a shift to higher angles in X-ray diffractometry. This prominent peak for diffraction at around 20° for the sodium alginate increased.

This result demonstrates the crosslinking reaction between sodium alginate (SA), covalent crosslinker (GrA) and ionic crosslinker ($CaCl_2$).

From this result, it was found that the amorphous region grew with the increase of PVA content. This suggests that the interaction between PVA and SA affects the increase of sodium alginate crystallinity and favors the amorphous structure of PVA.

Fig. 9b reveals the structure of the ALG3-PVA9-GO0.3 crosslinked membrane. From this characteristic peak, the amorphousness of membranes is mainly due to PVA rather than GO [55,56].

The diffraction peak at around 13° was present for non-crosslinked membranes when the solution of PVA of 3 to 9 wt.% was added to SA. It indicates the presence of crystallinity as reported by Yang et al. [57]. It is nonexistent in crosslinked membranes, which shows the lowest interaction between chloride calcium and sodium alginate membranes. This can be explained by the effect of time or concentration of crosslinking. Usually, as the crosslinking reaction progresses, the chain mobility of a polymer can be reduced by crosslinks. Thereby, the resulting semi-crystal peak was determined at $2\theta = 13°$. This peak corresponds to SA [58]. The wide range from 5° to 25° can give information on the presence of a component due to the presence of an amorphous structure. The amorphous signal was determined at $2\theta = 20°$. This typical and significant diffraction peak corresponds to PVA [59].

3.7. Fourier-transform infrared spectroscopy

The FTIR spectra of SA crosslinked and non-crosslinked membranes are shown in Fig. 10a and b, respectively.

The spectra of ALG3, ALG3-PVA3 and ALG3-PVA6 crosslinked membranes (Fig. 10a), shows a shift in the C=O peak from 1,616 cm^{-1} in the non-modified membrane to 1,623 cm^{-1} for the crosslinked membrane. This could result from a strong interaction between the carboxylate group and multivalent cations Ca^{2+} as a result of the crosslinking [60].

As can be seen, the hydrogen bonds were formed due to the interaction of the hydroxyl groups of PVA with the acetate group of SA. This can be related to the shift above and possibly to the addition of PVA, which reinforced the membranes to exhibit lower wave numbers than neat ALG3. In addition, the large band located at (1,933–3,600 cm^{-1}) corresponds to the stretching vibration of hydroxyl groups (–OH). This can confirm the presence of hydroxyl groups of SA [61,62]. Furthermore, the peak at 2,933 cm^{-1} is attributed to the O–H stretching vibration. This reveals that SA and PVA were interacting with strong hydrogen-bonds between the oxygen-containing group of PVA and SA chains [63].

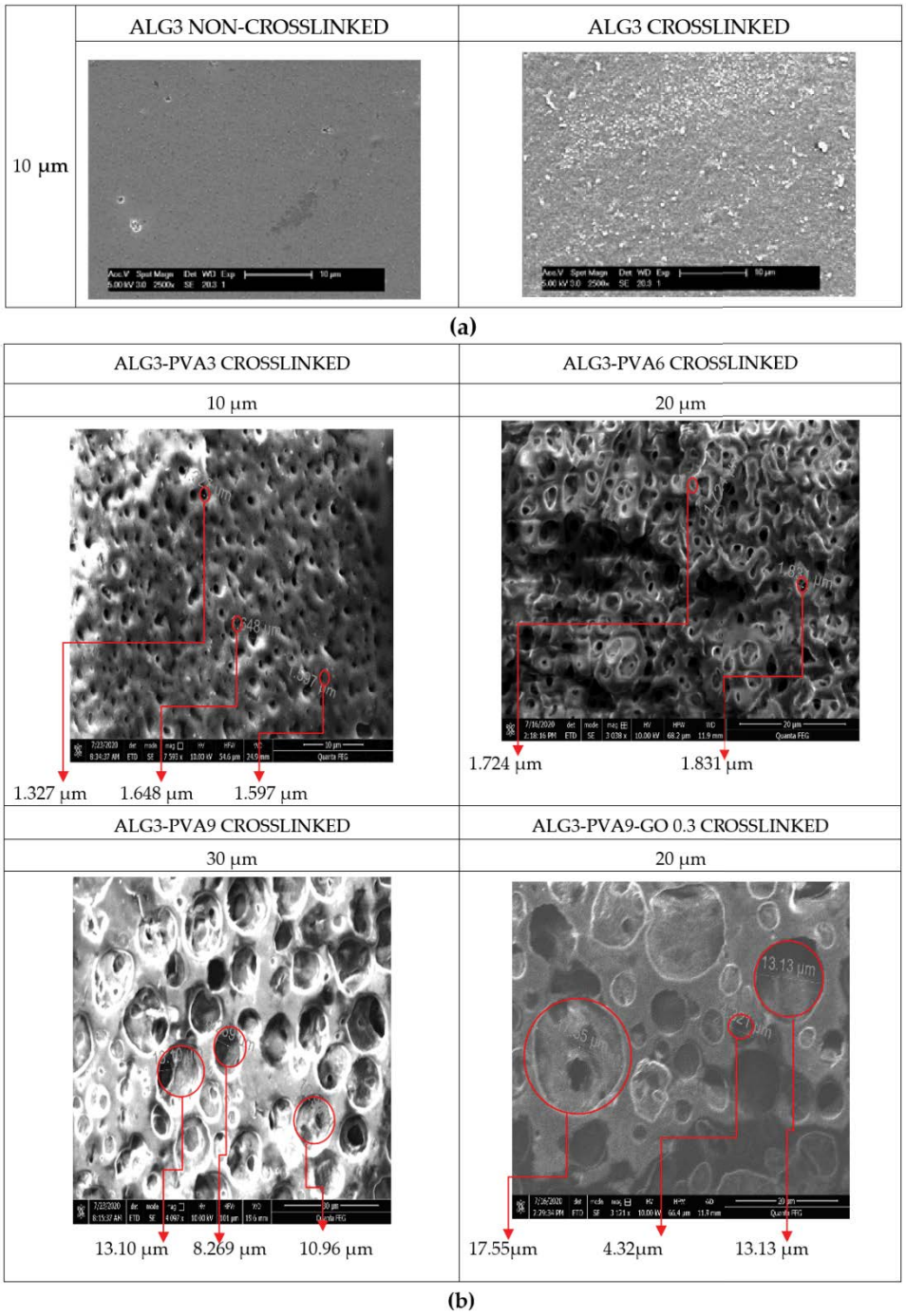

Fig. 8. (a) SEM micrographs of ALG3 of non-crosslinked and crosslinked membranes and (b) SEM micrographs of ALG3, ALG3-PVA3, ALG3-PVA6, ALG3-PVA9, ALG3-PVA9-GO0.3 crosslinked membranes.

However, the characteristic absorption bands at around 1,420 cm^{-1} are ascribed to the symmetries of carboxylate ions (COO^-) stretching vibration. For the crosslinked and non crosslinked membranes, the dominant peaks located at around 2,181 cm^{-1} are ascribed to the stretching vibration of C–O [64–67].

Additionally, a notable stretching deformation band of CH_2 groups was found at 1,339–1,420 cm^{-1}. These groups are regarded as functional groups in the chemical structure of PVA and ALG3-PVA [68]. The AlG3/ALG3-PVA3/ALG3-PVA6 crosslinked membranes and ALG3/ALG3-PVA6 non crosslinked membranes exhibited a characteristic band located at around 730 cm^{-1}. This band may be due to the stretching vibration (C–C), which monitored the intercalation of PVA and ALG3 molecules into GO by hydrogen and the bonding interactions between the hydroxyl groups of ALG3-PVA by GO hydroxyl groups [69]. The absorption band positioned at 1,086 cm^{-1} is imputed to the (C–O–C) stretching

vibration from the acetyl rings and ether linkages. The presence of this peak confirms the crosslinking of the alginate with glutaraldehyde through the formation of acetyl and ethyl linkages [70]. After crosslinking, the large band of hydroxyl groups (–OH) shifted to higher wavenumbers in comparison with non-crosslinked membranes. This shift would have taken part in the formation of acetyl bridges between the alcohol groups in the SA and the aldehydes in GrA.

The peak at around 2,200 cm^{-1} (C–H stretching) became more resolved and is ascribed to the aldehyde groups. In the crosslinking of the SA with GrA, only one aldehyde group is often used for two carboxyl groups from the SA

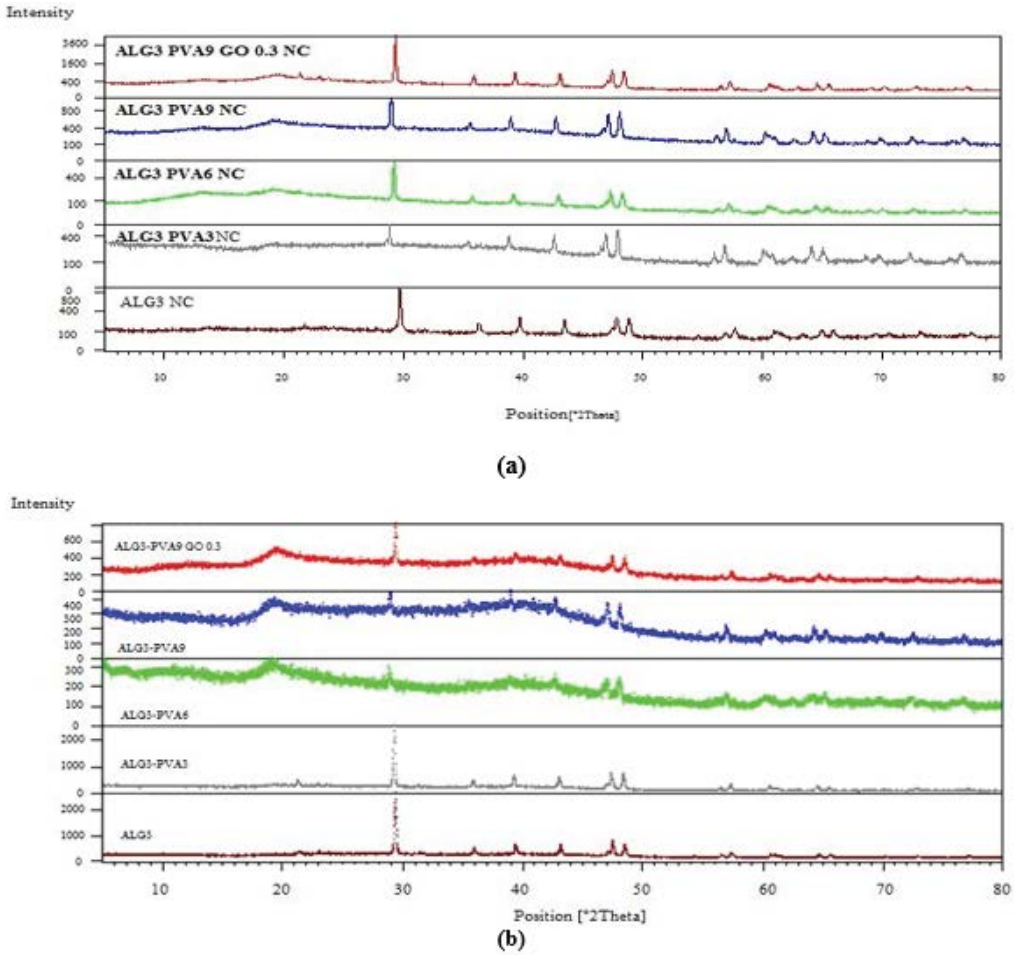

Fig. 9. X-ray diffractograms of (a) non-crosslinked and (b) crosslinked SA membranes.

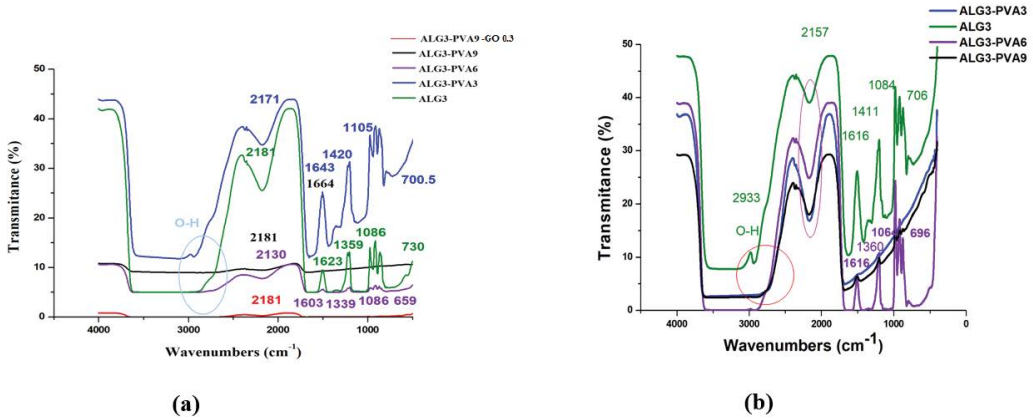

Fig. 10. FTIR spectra for (a) crosslinked sodium alginate (SA) membranes at 5 wt.% GrA and 2.5 wt.% $CaCl_2$ and (b) non-crosslinked sodium alginate (SA) membranes.

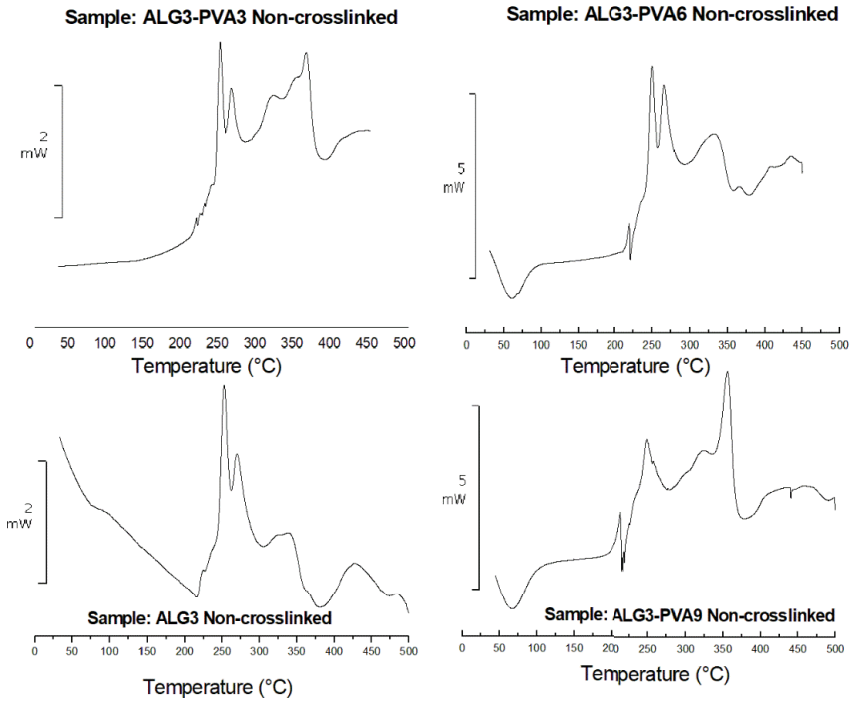

(a)

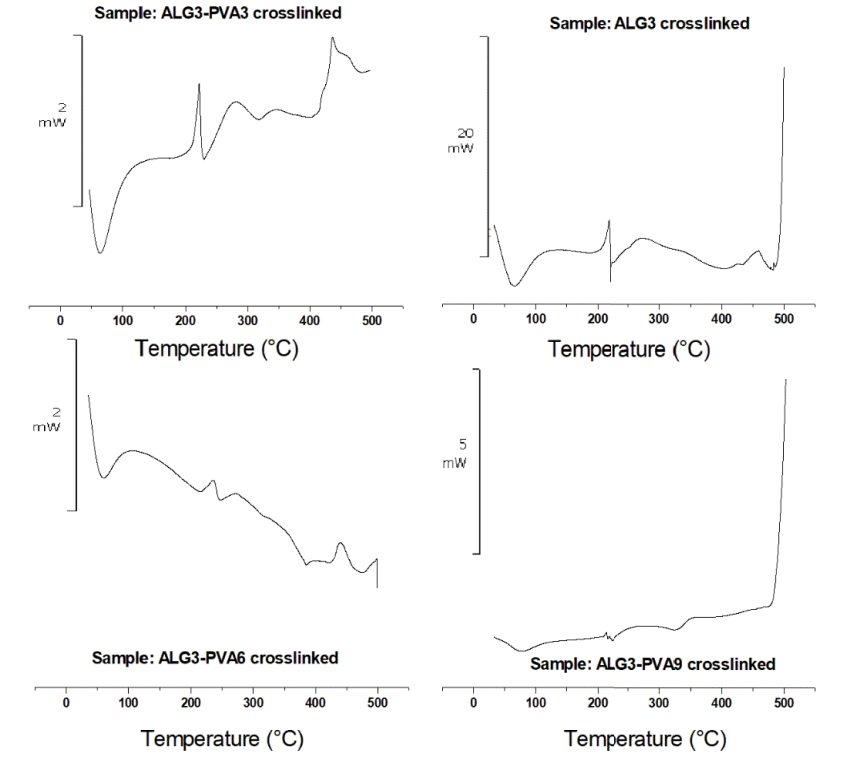

(b)

Fig. 11. DSC curves of the obtained (a) non-crosslinked and (b) crosslinked membranes ALG3; ALG3-PVA3; ALG3-PVA6; ALG3-PVA9.

[70]. On the other hand, the spectrum of ALG3 and ALG3-PVA6 of the non-crosslinked membrane is represented in Fig. 10b. It shows a prominent peak of C=O asymmetric stretching vibration of the free carboxylate ions at 1,616 cm^{-1} [71]. This confirms the observations of Bajdik et al. [72,73], which indicate that the bulk of the polymeric acid is in the protonated form.

3.8. Differential scanning calorimetry

The DSC curve of the obtained crosslinked membranes is presented in Fig. 11b. This figure shows an endothermic peak for the (ALG3, ALG3-PVA3, ALG3-PVA6) membranes at around 65°C. The (ALG3-PVA9) membrane presented a peak at around 75°C and two higher dehydration temperatures apex at 245°C and 325°C compared to other membranes. These endothermic peaks can be associated with the dehydration process of the samples. The exothermic peaks were observed for (ALG3, ALG3-PVA3, ALG3-PVA6, ALG3-PVA9) membranes at around 215°C–245°C, which may be associated with the presence of crosslinkers like $CaCl_2$ and GrA after crosslinking, granting more stability to the samples. These exothermic peaks can be associated with the sample degradation process.

The DSC curves of the obtained non-crosslinked membranes are presented in Fig. 11a. This figure shows an endothermic peak for the (ALG3-PVA6; ALG3-PVA9) membranes at around 65°C similar to crosslinked membranes. However, it was around 215°C for (ALG3) membrane. The endothermic peak at apex 380°C was observed for (ALG3 and ALG3-PVA9) membranes. However, the peak at apex 280°C was observed for (ALG3-PVA3) membrane.

Higher exothermic peak intensity was observed for all non-crosslinked membranes apex at 255°C. These peaks are attributed probably due to the decomposition of sodium alginate polymer of the samples which agree well with the value reported by Kong et al. [74].

3.9. Porosity measurement and pore size

The porosity of the different membranes was measured through a gravimetric method and the data are listed in Table 4. It can be seen that ALG3 exhibits a low porosity of about 19.2%, while the ALG3-PVA9-GO0.3 membrane exhibits the highest porosity (47.5%). Obviously, a more pronounced variation of this porosity is observed. This indicates that the addition of GO also has a synergistic effect in increasing the porosity. In the present work, the slightly enhanced porosity of the ALG3-PVA9-GO0.3 membrane is possibly attributed to the presence of some large pores on the top-surface.

Membranes with large pores tend to have a high flux, but low protein retention.

The pore size showed some increase from 1.65 to 1.83 and 13.1 μm for 3, 6 and 9 wt.% of PVA, respectively. However, it shifted back to a higher pore size for 0.3 wt.% GO in 17.6 μm. The effects of GO as a hydrophilic additive at the rate of exchange between solvent and non-solvent agents during phase inversion [75] can clarify this trend. The result of the crosslinked membranes is also shown in Table 4.

Table 4
Porosity of crosslinked sodium alginate membranes (ALG3/ALG3-PVA3/ALG3-PVA6/ALG3-PVA9/ALG3-PVA9-GO0.3)

Membrane	Porosity (%)
ALG3	19.2
ALG3-PVA3	27.3
ALG3-PVA6	38.1
ALG3-PVA9	47.5
ALG3-PVA9-GO0.3	51.7

The results showed that permeability is governed by the hydrophilicity of the membranes as well as their porosity. The high porosity of ALG3-PVA9-GO0.3 resulted in a higher flux and a lower rejection.

4. Conclusions

In this study, sodium alginate has demonstrated great potential as a biomaterial for membrane synthesis. Its application in ultrafiltration requires crosslinking. Crosslinking mediated by calcium chloride and glutaraldehyde was explored. Sodium alginate membranes were modified by enhancing the polyvinyl alcohol content and doping with graphene oxide to enhance their hydrophilicity and porosity.

The flux of the best membrane doped with graphene oxide (ALG3-PVA9-GO0.3) was 173.7 L h^{-1} m^{-2} and 128.9 L h^{-1} m^{-2} for pure water and solution containing BSA respectively at 2 bar.

The rejection for BSA is over 80%. However, the rejection of heavy metals with the best membrane has reached just around 30% at an optimum transmembrane pressure of 2 bar. The results of SEM show that there are synergistic effects between GO and PVA in enhancing the hydrophilicity, controlling the morphology, and increasing the porosity of the ALG3-PVA9-GO0.3 membrane. The DSC demonstrated endothermic peaks, which can be associated with the dehydration process of the samples. Exothermic peaks can reveal the presence of crosslinkers like $CaCl_2$ and GrA after crosslinking, granting more stability to the samples. In addition, they can be associated with the sample decomposition process of sodium alginate polymer of the samples. Alginate-based materials used in water treatment are likely to evolve considerably. Oceanic biopolymer membranes should be developed as an alternative to artificial polymer membranes.

Symbols

ε — Membrane porosity
W_1 — Weight of the wet membrane
W_2 — Weight of the dry membrane
M_w — Molecular weight
ρ — Density (g cm^{-3})
D_p — Polymer density
D_s — Solvent density
J_v — Permeation flux (L h^{-1} m^{-2})
V_p — Volume of the permeate water collected (L) in period of time t (h)

A — Effective membrane surface area (m^2)
Lp° — Permeability of solvent
η — Solvent viscosity
ΔP_m _ Transmembrane pressure
R_m _ Hydraulic membrane resistance
C_p _ Concentration of BSA, cobalt and copper in the permeate (g L^{-1})
C_f _ Concentration of BSA, cobalt and copper in the feed solution (g L^{-1})
R — Retention coefficients (%)

Declaration of competing interest

The authors declare no conflicts of interest.

Funding

This research received no external funding.

Acknowledgments

Asma Rhimi and Dorra Jellouli Ennigrou acknowledge the support provided by the core labs of Process Engineering for Sustainable Systems (ProcESS), KU Leuven.

The authors greatly thanks to the department of chemical Engineering, KU Leuven for their kind help and valuable assistance.

References

[1] M.R. Awual, A novel facial composite adsorbent for enhanced copper(II) detection and removal from wastewater, Chem. Eng. J., 266 (2015) 368–375.
[2] J.Z.Y. Tan, N.M. Nursam, F. Xia, M.-A. Sani, W. Li, X. Wang, R.A. Caruso, high-performance coral reef-like carbon nitrides: synthesis and application in photocatalysis and heavy metal ion adsorption, ACS Appl. Mater. Interfaces, 9 (2017) 4540–4547.
[3] S. Zheng, X. Li, X. Zhang, W. Wang, S. Yuan, Effect of inorganic regenerant properties on pharmaceutical adsorption and desorption performance on polymer anion exchange resin, Chemosphere, 182 (2017) 325–331.
[4] M.R. Awual, New type mesoporous conjugate material for selective optical copper(II) ions monitoring and removal from polluted waters, Chem. Eng. J., 307 (2017) 85–94.
[5] M.R. Awual, Solid phase sensitive palladium(II) ions detection and recovery using ligand based efficient conjugate nanomaterials, Chem. Eng. J., 300 (2016) 264–272.
[6] M.A. Abri, A. Dakheel, C. Tizaoui, N. Hilal, Combined humic substance and heavy metals coagulation, and membrane filtration under saline conditions, Desalination, 25 (2010) 46–50.
[7] N. Chitpong, S.M. Husson, High-capacity, nanofiber-based ion-exchange membranes for the selective recovery of heavy metals from impaired waters, Sep. Purif. Technol., 179 (2017) 94–103.
[8] U. Domanska, A. Rekawek, Extraction of metal ions from aqueous solutions using imidazolium based ionic liquids, J. Solution Chem., 38 (2009) 739–751.
[9] A. Kolbasov, S.S. Ray, A.L. Yarin, B. Pourdeyhimi, Heavy metal adsorption on solution-blown biopolymer nanofiber membranes, J. Membr. Sci., 530 (2017) 250–263.
[10] P. Wu, M. Imai, Novel Biopolymer Composite Membrane Involved with Selective Mass Transfer and Excellent Water Permeability, R.Y. Ning, Ed., Advancing Desalination, IntechOpen, Croatia, 2017, pp. 3157–3181, doi: 10.5772/50697.
[11] K. Kashima, M. Imai, Impact factors to regulate mass transfer characteristics of stable alginate membrane performed superior sensitivity on various organic chemicals, Procedia Eng., 42 (2012) 964–977.
[12] M.S. Mohy Eldin, A.E. Hashem, T.M. Tamer, A.M. Omer, M.E. Yossuf, M.M. Sabet, Development of crosslinked chitosan/alginate polyelectrolyte proton exchanger membranes for fuel cell applications, Int. J. Electrochem. Sci., 12 (2017) 3840–3858.
[13] I. Donati, S. Paoletti, Material Properties of Alginates, B.H.A. Rehm, Ed., Alginates: Biology and Applications, Springer-Verlag, Berlin, 2009, pp. 1–53.
[14] K.I. Draget, G.O. Phillips, P.A. Williams, Handbook of Hydrocolloids, Alginates, Woodhead Publishing Limited, Oxford Cambridge, 2009, pp. 1–902.
[15] C. Simpliciano, L. Clark, B. Asi, N. Chu, M. Mercado, S. Diaz, M. Goedert, M.M. Miremadi, Cross-linked alginate film pore size determination using atomic force microscopy and validation using diffusivity determinations, J. Surf. Eng. Mater. Adv. Technol., 3 (2013) 1–12.
[16] I.W. Cottrell, P. Kovacs, R.L. Davidson, Handbook of Water-Soluble Gums and Resins, Alginates, McGraw Hill Inc., New York, 1980, pp. 1–132.
[17] M.A. de Moraesa, D.S. Cocenza, F. da Cruz Vasconcellos, L.F. Fraceto, M.M. Beppu, Chitosan and alginate biopolymer membranes for remediation of contaminated water with herbicides, J. Environ. Manage., 131 (2013) 222–227.
[18] C.F. Huang, A.C. Huang, Y.F. Hsieh, F.J. Chu, T.J. Wan, The effects of magnetic nanoparticles embedded with SA/PVA and pH on chemical-mechanical polishing wastewater and magnetic particle regeneration and recycle, Water Resour. Ind., 18 (2017) 9–16.
[19] S.M.A. Soliman, A.M. Ali, M.W. Sabaa, Alginate-based hydrogel for water treatment, Desal. Water Treat., 94 (2017) 129–136.
[20] K.Y. Lee, D.J. Mooney, Alginate: properties and biomedical applications, Prog. Polym. Sci., 37 (2012) 106–126.
[21] C.Z. Bueno, A.M.A. Dias, H.J.C. de Sousa, M.E.M. Braga, A.M. Moraes, Control of the properties of porous chitosan-alginate membranes through the addition of different proportions of Pluronic F68, Mater. Sci. Eng., C, 44 (2014) 117–125.
[22] B. Ma, A. Qin, X. Li, X. Zhao, C. He, Structure and properties of chitin whisker reinforced chitosan membranes, Int. J. Biol. Macromol., 64 (2014) 341–346.
[23] T. Andersen, B.L. Strand, K. Formo, E. Alsberg, B.E. Christensen, Alginates as Biomaterials in Tissue Engineering, A.P. Rauter, T. Lindhorst, Eds., Carbohydrate Chemistry, Volume 37, The Royal Society of Chemistry, London, 2012, pp. 227–258.
[24] G. Orive, A.M. Carcaboso, R.M. Hernandez, A.R. Gascon, J.L. Pedraz, Biocompatibility evaluation of different alginates and alginate-based microcapsules, Biomacromolecules, 6 (2005) 927–931.
[25] Y. Yang, O.H. Campanella, B.R. Hamaker, G. Zhang, Z. Gu, Rheological investigation of alginate chain interactions induced by concentrating calcium cations, Food Hydrocolloids, 30 (2013) 26–32.
[26] G.T. Grant, E.R. Morris, D.A. Rees, P.J.C. Smith, D. Thom, Biological interactions between polysaccharides and divalent cations: the egg-box model, FEBS Lett., 32 (1973) 195–198.
[27] M. Al-Remawi, Sucrose as a crosslinking modifier for the preparation of calcium alginate films via external gelation, J. Appl. Sci., 12 (2012) 727–735.
[28] G.I. Olivas, G.V.B. Canovas, Alginate-calcium films: water vapor permeability and mechanical properties as affected by plasticizer and relative humidity, LWT-Food Sci. Technol., 41 (2008) 359–366.
[29] T.N. Julian, G.W. Radebaugh, S.J. Wisniewski, Permeability characteristics of calcium alginate films, J. Controlled Release, 7 (1988) 165–169.
[30] Y.A. Mørch, I. Donati, B.L. Strand, G.S. Braek, Effect of Ca^{2+}, Ba^{2+}, and Sr^{2+} on alginate microbeads, Biomacromolecules, 7 (2006) 1471–1480.
[31] O. Smidsrød, G.S. Bræk, Alginate as immobilization matrix for cells, Trends Biotechnol., 8 (1990) 71–78.
[32] R. Alfaro-Cuevas-Villanueva, A.R. Hidalgo-Vázquez, C. de Jesús Cortés Penagos, R. Cortés-Martínez, Thermodynamic,

kinetic, and equilibrium parameters for the removal of lead and cadmium from aqueous solutions with calcium alginate beads, Sci. World J., 2014 (2014) 1–9, doi: 10.1155/2014/647512.
[33] S.B. Kuila, S.K. Ray, Separation of benzene–cyclohexane mixtures by filled blend membranes of carboxymethyl cellulose and sodium alginate, Sep. Purif. Technol., 123 (2014) 45–52.
[34] J.M. Yang, N.C. Wang, H.C. Chiu, Preparation and characterization of poly (vinyl alcohol)/sodium alginate blended membrane for alkaline solid polymer electrolytes membrane, J. Membr. Sci., 457 (2014) 139–148.
[35] M.E. Nimni, D. Cheung, B. Strates, M. Kodama, K. Sheikh, Chemically modified collagen: a natural biomaterial for tissue replacement, J. Biomed. Mater. Res., 21 (1987) 741–771.
[36] Y. Li, H. Jia, Q. Cheng, F. Pan, Z. Jiang, Sodium alginate–gelatin polyelectrolyte complex membranes with both high water vapor permeance and high permselectivity, J. Membr. Sci., 375 (2011) 304–312.
[37] E.A. Kamoun, E.R.S. Kenawy, T.M. Tamer, M.A. El-Meligy, M.S. Mohy Eldin, Poly(vinyl alcohol)-alginate physically crosslinked hydrogel membranes for wound dressing applications: characterization and bio-evaluation, Arabian J. Chem., 8 (2015) 38–47.
[38] K. Cao, Z. Jiang, J. Zhao, C. Zhao, C. Gao, F. Pan, B. Wang, X. Cao, J. Yang, Enhanced water permeation through sodium alginate membranes by incorporating graphene oxides, J. Membr. Sci., 469 (2014) 272–283.
[39] J.H. Chen, Q.L. Liu, S.R. Hu, J.C. Ni, Y.S. He, Adsorption mechanism of Cu(II) ions from aqueous solution by glutaraldehyde crosslinked humic acid-immobilized sodium alginate porous membrane adsorbent, J. Chem. Eng., 173 (2011) 511–519.
[40] J.H. Chen, H.T. Xing, H.X. Guo, G.P. Li, W. Weng, S.R. Hu, Preparation, characterization and adsorption properties of a novel 3-aminopropyltriethoxysilane functionalized sodium alginate porous membrane adsorbent for Cr(III) ions, J. Hazard. Mater., 248–249 (2013) 285–294.
[41] Y.Q. Dong, L.L. Zhang, J.N. Shen, M.Y. Song, H.L. Chen, Preparation of poly(vinyl alcohol)-sodium alginate hollow-fiber composite membranes and pervaporation dehydration characterization of aqueous alcohol mixtures, Desalination, 193 (2006) 202–210.
[42] S. Mokhtarzadeh, F. Hakimpour, R. Sarvari, S. Agbolaghi, Y. Mansourpanah, Nanocomposite membranes based on sodium alginate/poly(ε-caprolactone)/graphene oxide for methanol, ethanol and isopropanol dehydration via pervaporation, Polym. Bull., 77 (2019) 1–21.
[43] S. Mallakpour, V. Behranvand, Chapter 10 – Green Hybrid Nanocomposites from Metal Oxides, Poly(Vinyl Alcohol) and Poly(Vinyl Pyrrolidone): Structure and Chemistry, V. Kumar Thakur, M. Kumari Thakur, R. Kumar Gupta, Eds., Hybrid Polymer Composite Materials: Structure and Chemistry, Woodhead Publishing, 2017, pp. 263–289, doi: 10.1016/B978-0-08-100791-4.00010-0.
[44] S. Mallakpour, M. Dinari, Nanocomposites of poly(vinyl alcohol) reinforced with chemically modified Al_2O_3: synthesis and characterization, J. Macromol. Sci. Part B Phys., 52 (2013) 1651–1661.
[45] S. Mallakpour, M. Zhiani, A. Barati, H. Rostami, Improving the direct methanol fuel cell performance with poly(vinyl alcohol)/titanium dioxide nanocomposites as a novel electrolyte additive, Int. J. Hydrogen Energy, 38 (2013) 12418–12426.
[46] R.Y.M. Huang, Pervaporation Membrane Separation Processes, Elsevier Science, Amsterdam, New York, 1991, pp. 53–278.
[47] D. Han, L. Yan, W. Chen, W. Li, Preparation of chitosan/graphene oxide composite film with enhanced mechanical strength in the wet state, Carbohydr. Polym., 83 (2011) 653–658.
[48] T. Kobayashi, M. Yoshimoto, K. Nakao, Preparation and characterization of immobilized chelate extractant in PVA gel beads for an efficient recovery of copper(II) in aqueous solution, Ind. Eng. Chem. Res., 49 (2010) 11652–11660.
[49] N.W. Choi, M. Cabodi, B. Held, J.P. Gleghorn, L.J. Bonassar, A.D. Strook, Microfluidic scaffolds for tissue engineering, Nat. Mater., 6 (2007) 908–915.
[50] A.W. Chan, R.J. Neufeld, Tuneable semi-synthetic network alginate for absorptive encapsulation and controlled release of protein therapeutics, Biomaterials, 31 (2010) 9040–9047.
[51] R.H. Li, D.H. Altreuter, F.T. Gentile, Transport characterization of hydrogel matrices for cell encapsulation, Biotechnol. Bioeng., 50 (1996) 365–373.
[52] M. Hepel, L. Dentrone, Controlled incorporation of heavy metals from aqueous solutions and their electrorelease using composite polypyrrole films, Electroanalysis, 8 (1996) 996–1005.
[53] M. Chan, S. Ng, Effect of membrane properties on contact angle, AIP Conf. Proc., 6 (2016) 020035–1/020035–6.
[54] Y. Yu, G. Zhang, L. Ye, Preparation and adsorption mechanism of polyvinyl alcohol/graphene oxide sodium alginate nanocomposite hydrogel with high Pb(II) adsorption capacity, J. Appl. Polym. Sci., 136 (2019) 47318, doi: 10.1002/app.47318.
[55] H. Zheng, J. Yang, S. Han, The synthesis and characteristics of sodium alginate/graphene oxide composite films crosslinked with multivalent cations, J. Appl. Polym. Sci., 133 (2016) 1–7.
[56] H. Liu, P. Bandyopadhyay, N.H. Kim, B. Moon, J.H. Lee, Surface modified graphene oxide/poly(vinyl alcohol) composite for enhanced hydrogen gas barrier film, Polym. Test., 50 (2016) 49–56.
[57] G. Yang, L. Zhang, T. Peng, W. Zhong, Effects of Ca^{2+} bridge cross-linking on structure and pervaporation of cellulose/alginate blend membranes, J. Membr. Sci., 175 (2000) 53–60.
[58] S. Jana, M.K. Trivedi, R.M. Tallapragada, A. Branton, D. Trivedi, G. Nayak, R.K. Mishra, Characterization of physicochemical and thermal properties of chitosan and sodium alginate after biofield treatment, Pharm. Anal. Acta, 6 (2015) 2135–2435.
[59] G. Attia, M.F.H. Abd El-kader, Structural optical and thermal characterization of PVA/2HEC polyblend films, Int. J. Electrochem. Sci., 8 (2013) 5672–5687.
[60] S.B. Hua, H.Z. Ma, X. Li, H.X. Yang, A.Q. Wang, pH sensitive sodium alginate/poly(vinyl alcohol) hydrogel beads prepared by combined Ca^{2+} crosslinking and freeze-thawing cycles for controlled release of diclofenac sodium, Int. J. Biol. Macromol., 46 (2010) 517–523.
[61] W.M. Algothmi, N.M. Bandaru, Y. Yu, J.G. Shapter, A.V. Ellis, Alginate-graphene oxide hybrid gel beads: an efficient copper adsorbent material, J. Colloid Interface Sci., 397 (2013) 32–38.
[62] L. Sun, B. Fugetsu, Graphene oxide captured for green use: influence on the structures of calcium alginate and macroporous alginic beads and their application to aqueous removal of acridine orange, Chem. Eng. J., 240 (2014) 565–573.
[63] V.K. Malesu, D. Sahoo, P.L. Nayak, Chitosan–sodium alginate nanocomposites blended 258 with cloisite 30B as a novel drug delivery system for anticancer drug curcumin, Int. J. Appl. Biol. Pharm., 2 (2011) 402–411.
[64] Y.Q. He, N.N. Zhang, Q.J. Gong, H.X. Qiu, W. Wang, Y. Liu, J.P. Gao, Alginate/graphene oxide fibers with enhanced mechanical strength prepared by wet spinning, Carbohydr. Polym., 88 (2012) 1100–1108.
[65] C.L. Jiao, P.G. Xiong, J. Tao, S.J. Xu, D.S. Zhang, H. Lin, Y.Y. Chen, Sodium alginate/graphene oxide aerogel with enhanced strength-toughness and its heavy metal adsorption study, Int. J. Biol. Macromol., 83 (2016) 133–141.
[66] S.Q. Gong, Z.J. Jiang, P.H. Shi, J.C. Fan, Q.J. Xu, Y.L. Min, Noble-metal-free heterostructure for efficient hydrogen evolution in visible region: molybdenum nitride/ultrathin graphitic carbon nitride, Appl. Catal., B, 238 (2018) 318–327.
[67] Z.Q. Wang, P.X. Jin, M. Wang, G.H. Wu, J.Y. Sun, Y.J. Zhang, C. Dong, A.G. Wu, Highly efficient removal of toxic Pb^{2+} from wastewater by an alginate-chitosan hybrid adsorbent, Technol. Biotechnol., 93 (2018) 2691–2700.
[68] M. Xie, F. Zhang, L. Liu, Y. Zhang, Y. Li, H. Li, J. Xie, Surface modification of graphene oxide nanosheets by protamine sulfate/sodium alginate for anti-cancer drug delivery application, Appl. Surf. Sci., 440 (2018) 853–860.
[69] S. Amiri, A. Asghari, V. Vatanpour, M. Rajabi, Fabrication and characterization of a novel polyvinyl alcohol-graphene-sodium alginate nanocomposite hydrogel blended PES nanofiltration

membrane for improved water purification, Sep. Purif. Technol., 250 (2020) 117216, doi: 10.1016/j.seppur.2020.117216.
[70] C.K. Yeom, K.H. LEE, Characterization of sodium alginate membrane crosslinked with glutaraldehyde in pervaporation separation, J. Appl. Polym. Sci., 67 (1998) 209–219.
[71] C. Liu, H. Liu, T. Xiong, A. Xu, B. Pan, K. Tang, Graphene oxide reinforced alginate/PVA double network hydrogels for efficient dye removal, Polymers, 10 (2018) 1–14.
[72] J. Bajdik, Z. Makai, O. Berkesi, K. Suvegh, T. Marek, I. Eros, K. Pintye-Hodi, Study of the effect of lactose on the structure of sodium alginate films, Carbohydr. Polym., 77 (2009) 530–535.
[73] G. Socrates, Infrared and Raman Characteristic Group Frequencies: Tables and Charts, 3rd ed., John Wiley and Sons Ltd., England, 2001, 366 pp.
[74] Q.S. Kong, B.B. Wang, Q. Ji, Y.Z. Xia, Z.X. Guo, J. Yu, Thermal degradation and flame retardancy of calcium alginate fibers, Chin. J. Polym. Sci., 27 (2009) 807–812.
[75] M. Khajouei, M. Najafi, S.A. Jafari, Development of ultrafiltration membrane via in-situ grafting of nano-GO/PSF with anti-biofouling properties, Chem. Eng. Res. Des., 142 (2019) 34–43.